

Significant increase in sensitive volume of a gravitational wave search upon including higher harmonics

Ajit Kumar Mehta,¹ Digvijay Wadekar,^{2,3} Javier Roulet,¹ Isha Anantpurkar,¹ Tejaswi Venumadhav,^{1,4} Jonathan Mushkin,⁵ Barak Zackay,⁵ Matias Zaldarriaga,³ and Tousif Islam^{6,7}

¹*Department of Physics, University of California at Santa Barbara, Santa Barbara, CA 93106, USA*

²*Department of Physics and Astronomy, Johns Hopkins University, 3400 N. Charles Street, Baltimore, Maryland, 21218, USA*

³*School of Natural Sciences, Institute for Advanced Study, 1 Einstein Drive, Princeton, NJ 08540, USA*


⁴*International Centre for Theoretical Sciences, Tata Institute of Fundamental Research, Bangalore 560089, India*

⁵*Department of Particle Physics & Astrophysics, Weizmann Institute of Science, Rehovot 76100, Israel*

⁶*Kavli Institute for Theoretical Physics, University of California Santa Barbara, Santa Barbara, CA 93106*

⁷*Theoretical AstroPhysics Including Relativity and Cosmology, California Institute of Technology, Pasadena, California, USA*

(Dated: January 31, 2025)

Most gravitational wave searches to date have included only the quadrupole mode in their search templates. Here, we demonstrate that incorporating higher harmonics improves the search sensitive volume for detecting binary black hole mergers, challenging the conclusion of previous studies. Using the IAS – HM detection pipeline^a [1], and the simulated (injection) signals from the LIGO-Virgo-Kagra (LVK) collaboration, we quantify the improvement in sensitivity due to the inclusion of higher harmonics. This improvement is significant for systems with higher mass ratios and larger total masses, with gains in sensitivity even exceeding 100% at certain high masses. We also show that, due to using a marginalized detection statistic, the IAS – HM pipeline performs roughly as well as its quadrupole-mode-only counterpart even for equal mass-ratio mergers, and its sensitive volume is either better than or comparable to that of the individual LVK pipelines. 

INTRODUCTION

The LIGO, Virgo and KAGRA detectors currently [2–4] provide strain data that contain gravitational wave (GW) signals from mergers of compact binary systems, such as binary black holes (BBHs). Multiple GW detection pipelines, developed both within and outside the LIGO-Virgo-KAGRA (LVK) collaboration [1, 5–18], analyze this data to identify the signals. In the first three observing runs, approximately 100 compact binary mergers have been detected [15, 17, 19, 20]. These detections have significantly advanced our understanding of astrophysics [15, 21, 22] and fundamental physics [23].

Currently, most detections have been made using search templates that include only the dominant harmonic (the 22-mode) of GW signals [5–17]. However, signals with substantial contributions from higher modes (HM), such as those emitted by BBH systems with high mass ratios or high total masses (particularly in the intermediate-mass black holes (IMBH) range), may be missed by these 22-mode-only pipelines [24–36]. Detecting such systems can significantly improve our knowledge of the diverse formation channels of BBHs [37–53], and physics of the pair-instability mass gap [54–60]. The lack of IMBH detections at the moment leaves their formation mechanisms highly uncertain and poorly understood. [61–64].

Incorporating HM in search templates introduces two competing effects: on one hand, it increases the captured signal-to-noise ratio (SNR), while on the other hand, it causes an increase in background noise and degradation of false-alarm rate (FAR) of detected signals (as noise can increasingly mimic real signals due to addition of extra degrees of freedom introduced by HM in the templates) [27, 33, 65]. Due to this trade-off, earlier studies concluded that including HMs in searches was unlikely to enhance the overall detection sensitivity of compact binary mergers [27, 33].

We recently developed a new efficient *mode-by-mode filtering* method to include HM into a search pipeline (see Fig. 1 of [1]). We matched-filter the strain data with different normalized harmonics and then combine the residual signal-to-noise timeseries [24]. This has two advantages: (*i*) the matched-filtering cost becomes linearly proportional to the number of HM used (instead of increasing by a factor of ~ 100 if a brute-force method is used [32, 33]); (*ii*) it allows for efficient marginalization over the extra degrees of freedom corresponding to HM (namely the binary inclination and the initial reference phase). It is worth noting that the mode-by-mode filtering method can also be used for efficient parameter estimation of the detected binaries [66, 67]. We leave the details of our detection statistics and template banks to Refs. [1] and [24] respectively.

Our goal in this paper is to precisely quantify increase/decrease in the sensitive volume upon introducing HM (using a mode-by-mode filtering method) in the search pipeline. We estimate the sensitive volume of the

^a The IAS – HM pipeline is publicly available at <https://github.com/JayWadekar/gwIAS-HM>

IAS – HM pipeline^a by analyzing simulated signals (injections) made publicly available by the LVK collaboration on Zenodo corresponding to the second part of the third observing run (O3b) [68]. We also estimate the sensitivity of the IAS – HM pipeline in its 22-mode-only limit (referred to as the IAS – 22 pipeline). This allows us to understand the improvement in sensitivity volume solely due to the inclusion of HM.

We had performed the first search accounting for HM throughout the BBH parameter space in Ref. [20] (see also Ref. [33]). Using the IAS – HM pipeline, we had found ~ 10 new BBH mergers, most of which had median primary masses¹ exceeding $60 M_\odot$ in the source frame [20]. As we discuss below, this mass range aligns with where we observe significant improvements in detection sensitivity volume upon including HM, adding more credibility to our previously-reported detections.

Our results are in Figs. 1 and 2. For low-mass BBH systems, the sensitivity either remains roughly the same or shows a modest improvement. The improvement becomes more pronounced as the mass ratio and primary mass (or the total mass) increase. For reference, for IMBH binaries with a mass ratio $q = 1/4$, we find that HM enhance the sensitivity by $\sim 15\% - 150\%$ for primary mass between $\sim [100, 250] M_\odot$.

METHOD

The expected number of detections, N_{det} , from a given pipeline can be expressed as:

$$N_{\text{det}} = \int \left(\frac{d^3 N}{dt_s dV_c d\theta} \right) \frac{dV_c}{dz} \frac{dt_s}{dt} p(\text{det}|\theta, z) dt d\theta dz \quad (1)$$

Here, the quantity inside the parenthesis describes the number of compact binary mergers per unit source-frame time (dt_s), per unit comoving volume (dV_c) for a given set of intrinsic source parameters $\theta = (m_1^s, m_2^s, \vec{s}_1, \vec{s}_2)$. The parameters $m_{1,2}^s$ denote the primary and secondary mass of the compact binary merger in the source-frame with $m_2^s \leq m_1^s$, and $\vec{s}_{1,2}$ represent the component spin vectors. The term $p(\text{det}|\theta, z)$ denotes the probability that a merger signal with parameters (θ, z) is detected by the considered pipeline. The observer-frame time (dt) relates to the source-frame time (dt_s) via $dt = (1 + z) dt_s$, accounting for cosmic time dilation.

The term inside the parenthesis can be further decomposed as:

$$\frac{d^3 N}{dt_s dV_c d\theta} = R(z) p(\theta) \quad (2)$$

where $R(z)$ is the merger rate density as a function of redshift, and $p(\theta)$ is the astrophysical probability distribution over the intrinsic source parameters θ . The merger rate density can be parameterized as $R(z) = R_0 f(z)$, where R_0 is the local merger rate density, i.e., at $z = 0$ and $f(z)$ accounts for the redshift evolution of the rate density.

Substituting these definitions into Eq. (1), the expected number of detections can be written as:

$$N_{\text{det}} = R_0 \int f(z) \frac{1}{1+z} \frac{dV_c}{dz} p(\theta) p(\text{det}|\theta, z) dt d\theta dz \quad (3)$$

The detection sensitivity volume is defined as,

$$\overline{VT} = \int f(z) \frac{1}{1+z} \frac{dV_c}{dz} p(\theta) p(\text{det}|\theta, z) dt d\theta dz \quad (4)$$

so that $N_{\text{det}} = R_0 \overline{VT}$. Thus, \overline{VT} represents the comoving volume-time accessible to the detector, weighted by astrophysical, cosmological, and detector-specific factors.

To compute \overline{VT} from Eq. (4), we use a Monte Carlo integral over found injections [69]:

$$\overline{VT} \simeq \frac{T_{\text{obs}}}{N_{\text{draw}}} \sum_{j=1}^{N_{\text{found}}} \frac{f(z_j) \frac{1}{1+z_j} \frac{dV_c(z_j)}{dz} p(\theta_j)}{\pi_{\text{draw}}(\theta_j, z_j)} \quad (5)$$

where T_{obs} is the observation time of the dataset analyzed, N_{draw} is the number of injections generated from the sampling distribution π_{draw} , and N_{found} is the number of injections detected by the pipeline. The Monte Carlo estimate weights each found injection by the inverse of the sampling probability π_{draw} , ensuring unbiased sensitivity volume estimates.

The uncertainty in \overline{VT} is evaluated using the bootstrap method. Specifically, we resample the detected injections (the quantity inside the sum in Eq. (5)) with replacement, generating multiple bootstrap samples of size N_{found} . For each bootstrap sample, we compute the sensitivity volume. The mean of these bootstrap samples is used as the final estimate of \overline{VT} , while the 90% confidence interval from the bootstrap distribution provides the error bars. This approach ensures a robust characterization of the uncertainty in the sensitivity volume. In all results presented in this paper, we use the bootstrap mean as the representative value of \overline{VT} , and the 90% confidence interval as the associated error bar. As we would expect, \overline{VT} closely follows a normal distribution with a variance that can be expressed as:

$$\sigma^2 = \frac{\overline{VT}^2}{N_{\text{eff}}} \quad (6)$$

where N_{eff} is the effective number of detected injections, accounting for the weighting by π_{draw} . An expression for N_{eff} can be found in Eq. 9 of Ref. [70].

¹ The heavier masses of the binary components.

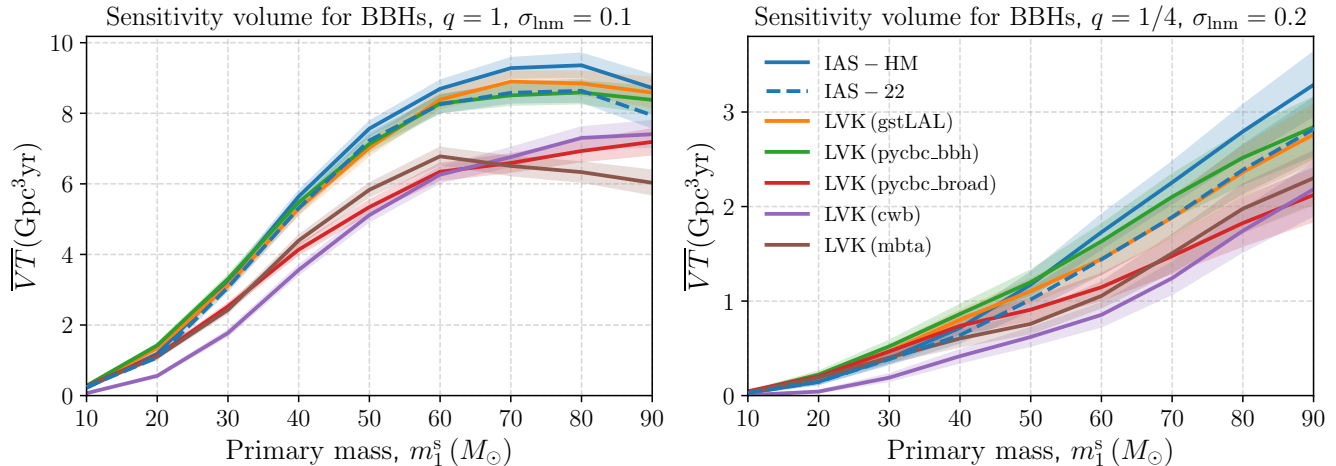


FIG. 1: Detection sensitivity volume and its measurement uncertainty for the IAS and LVK search pipelines, using a detection criterion of $p_{\text{astro}} > 0.5$. The x -axis represents the mean values of the log-normal distributions assumed for the primary masses in the source frame (see Eq. (8)). **Left panel:** For $q = 1$. The IAS pipeline with HM (IAS – HM) performs equally well as its 22-only counterpart (IAS – 22) and demonstrates performance that is roughly comparable to, the individual LVK pipelines. **Right panel:** For $q = 1/4$. The IAS – HM pipeline performs significantly better than both the 22-mode counterpart IAS – 22, as well as the individual LVK pipelines towards the higher masses. This is expected for lower mass ratios and larger total masses, where the contributions from HM to the signals become increasingly significant. Note that, for both panels, the IAS pipelines were run only on Hanford and Livingston detectors (including Virgo will further improve the IAS \overline{VT} estimates).

In this work, we calculate \overline{VT} for the IAS pipelines and compare it with the \overline{VT} of various LVK pipelines. We use the injection datasets made publicly available by the LVK collaboration on Zenodo [68]. We focus on the observing run O3b throughout this paper. The injection datasets include:

- A BBH injection set, with source-frame component masses in the range $[2, 100] M_{\odot}$. The primary mass follows a power-law distribution, $p(m_1^s) \propto (m_1^s)^{\alpha}$, where the exponent $\alpha = -2.35$. The secondary mass (m_2^s) is drawn from a conditional power-law distribution with exponent $\alpha = 1$, conditioned on m_1^s . Spins are isotropically distributed in direction and uniformly in magnitude. The redshift distribution in Eq. (4) is given by $f(z) = (1 + z)$ with a maximum redshift $z_{\text{max}} = 1.9$.
- An IMBH binary injection set, with primary masses between $[90, 600] M_{\odot}$ and secondary masses in the range $[10, 600] M_{\odot}$. Both the primary mass distribution, $p(m_1^s)$, and the conditional distribution of the secondary mass, $p(m_2^s|m_1^s)$, follow a power-law with exponent $\alpha = -1$. The spin distribution is the same as the BBH injection set. The redshift distribution assumes no evolution with $f(z) = 1$, and a maximum redshift $z_{\text{max}} = 2.5$.

For each injection dataset, we evaluate \overline{VT} of the IAS pipelines by injecting signals into the O3b data from the Hanford and Livingston detectors. For the BBH injection set, we apply the detection criterion $p_{\text{astro}} > 0.5$

(where p_{astro} refers to the probability of a trigger being astrophysical in origin, as opposed to a noise artifact), consistent with thresholds used in real LVK and IAS searches. For the IMBH dataset, however, only IFAR (i.e., FAR^{-1}) values are provided (and not p_{astro}), and furthermore, only the results from one of the LVK pipelines (pycbc.bbh) are reported. Therefore, for the IMBH dataset, we use $\text{IFAR} > 1$ year as the detection criterion and compare our results only with pycbc.bbh.

It is important to note that the IAS pipelines currently analyze data from only from the Hanford and Livingston detectors, whereas LVK pipelines incorporate Virgo data as well. Including additional detectors enhances sensitivity volume. Thus, while comparing \overline{VT} between the IAS and LVK pipelines, this is an important point to keep in mind. We aim to include also the Virgo data in future IAS analysis papers.

A key objective of this work is to evaluate the improvement in \overline{VT} due to HM. To achieve this, we compute the ratio $\overline{VT}_{\text{HM}}/\overline{VT}_{22}$, also expressed as the fractional gain:

$$\Delta\overline{VT} = \frac{\overline{VT}_{\text{HM}}}{\overline{VT}_{22}} - 1 \quad (7)$$

where $\overline{VT}_{\text{HM}}$ is the sensitivity volume of the IAS – HM pipeline, and \overline{VT}_{22} corresponds to the IAS – 22 pipeline. We estimate the uncertainty in $\Delta\overline{VT}$ using the bootstrap method as explained before. By systematically evaluating $\Delta\overline{VT}$ across different masses (as discussed in the following section), we identify regions of the parameter space where the inclusion of higher harmonics significantly enhances the sensitivity volume.

RESULTS AND DISCUSSION

Sensitivity volume for BBH injection set

In Fig. 1, we present the sensitivity volume (\overline{VT}) and its associated measurement uncertainties for the IAS and

$$p(m_1^s, m_2^s) = \begin{cases} \frac{c}{2\pi\sigma_{\text{lnm}}^2 m_1^s m_2^s} \exp\left(-\frac{1}{2} \frac{(\log m_1^s - \log M_1)^2}{\sigma_{\text{lnm}}^2}\right) \exp\left(-\frac{1}{2} \frac{(\log m_2^s - \log M_2)^2}{\sigma_{\text{lnm}}^2}\right), & \text{for } m_2^s < m_1^s, \\ 0, & \text{otherwise.} \end{cases} \quad (8)$$

For spins and other parameters, we adopt the same distributions as the injection set, i.e., π_{draw} .

The x -axes in Fig. 1 represent the mean values (M_1) of the log-normal distribution for the primary mass. We use a fixed variance of $\sigma_{\text{lnm}} = 0.1$ in the left panel. In the right panel, however, we use a larger width ($\sigma_{\text{lnm}} = 0.2$) to maintain a sufficiently large N_{eff} , ensuring the smoothness of curves as well as upper bounds on the error bars. In the left panel, the mean mass ratio ($q = M_2/M_1$) is held constant at 1, so the x -axis also corresponds to half the mean total source-frame mass. This figure is derived from the BBH injection set, which spans component masses up to $100 M_\odot$. To account for this hard cut-off, we appropriately re-normalize the log-normal mass distributions. To ensure sufficient statistical precision of \overline{VT} , characterized by N_{eff} , we restrict the x -axis to below $90 M_\odot$. We use $p_{\text{astro}} > 0.5$ as the detection criterion following the approach of other pipelines [19].

Overall trends: Let us first discuss the overall trends seen across all the pipelines. All the pipelines exhibit an initial increase in \overline{VT} with the total mass of the binary mergers, followed by a plateau, and an eventual decline at higher masses (which is seen more clearly in Fig. 2). This behavior is primarily due to the fact that the amplitude of GW signals increases with the total mass, enhancing detectability. For reference, the amplitude scales as $|h| \propto \mathcal{M}^{5/6}$ in the inspiral-dominated regime, where $\mathcal{M} = M_{\text{tot}} \left(\frac{q}{(1+q)^2}\right)^{3/5}$ is the chirp mass. However, beyond a certain total mass ($\sim 80 M_\odot$ for most pipelines), the dominant GW frequencies shift out of the detector's sensitive band, reducing the effective detection volume. Interestingly, this flattening is not observed in the right panel of Fig. 1, which presents results for $q = 1/4$. At lower mass ratios, the increased signal duration (and the corresponding higher number of cycles) allows the GW signals to remain within the detector's sensitive frequency band for larger primary masses (for reference, roughly, $f_{\text{merger}} \propto M_{\text{tot}}^{-1}$ for a non-spinning case and thus goes up with lower q). Nevertheless, the \overline{VT} for $q = 1/4$ is generally lower than that for $q = 1$, as the GW

LVK pipelines as a function of the primary source-frame mass (m_1^s). For this analysis and throughout the work, we assume a log-normal distribution for the primary and secondary component masses in the astrophysical prior $p(m_1^s, m_2^s)$ in Eq. (5), consistent with the LVK analysis in Ref. [19]. Specifically,

signal strength decreases with lower mass ratios. These observations underscore the complex interplay between signal morphology, mass ratio, and detector sensitivity in determining detection volumes across varying parameter spaces.

Comparison of 22+HM and 22-only pipelines: The IAS – HM pipeline includes the modes: (2,2), (3,3) and (4,4). The (2,2)-only limit of the pipeline is labeled as IAS – 22. It is worth noting that the IAS – 22 case is an improved version of the 22-only IAS pipeline used in our previous searches in [11, 17], see the supplemental material for more details.

For $q = 1$, IAS – HM case exhibits roughly similar sensitivity as IAS – 22. This result is noteworthy because earlier studies have suggested that the inclusion of HM might lead to diminished sensitivity for $q \sim 1$ due to an increased FAR [27]. This worry primarily stemmed from the fact that $q \sim 1$ systems do not gain much in SNR due to HM, but the searches catch additional background due to the additional degrees of freedom in the HM templates. HM do boost the detection of nearly edge-on and asymmetric mass-ratio systems, but such systems have a much smaller observable volume to begin with, and thus the \overline{VT} of the overall search could be compromised.

We designed our marginalized detection statistic in Refs. [1, 67] to limit the increase in search background due to HM. For example, while performing the marginalization integral over inclination, we add smaller weights to the edge-on configurations instead of face-on configuration (to account for the difference in their observable volume). Similarly, the different binary mass-ratio configurations are also weighed by their observable volume. This helps in preserving the sensitivity of the search in $q = 1$ case.

For $q = 1/4$, the IAS – HM pipeline exhibits a marked improvement in sensitivity volume with increasing primary mass, outperforming both the IAS – 22 and other LVK pipelines. This enhancement can be attributed to the growing contribution of HM to the signal's power within the detector's sensitive frequency band as the primary mass increases (see Fig. 3 of [24]). Beyond

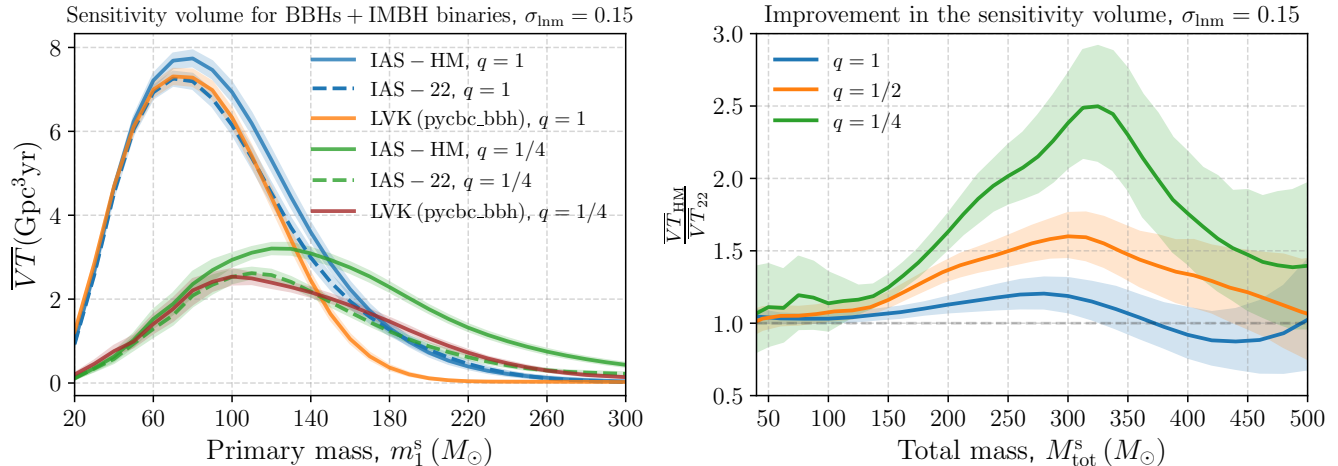


FIG. 2: Same as Fig. 1, but including the injection set for IMBH binaries in addition to the lower-mass BBH set. **Left panel:** Detection sensitivity volumes for two cases: $q = 1$ and $q = 1/4$. The public LVK IMBH binary injection set only contains results for the `pycbc_bbh` pipeline and does not include p_{astro} values. We thus use $\text{IFAR} > 1$ as the detectability criterion for both the injection sets in this plot and only compare with `pycbc_bbh`. The IAS – HM pipeline has comparable or higher sensitivity compared to IAS – 22 throughout the parameter space. Interestingly, for $m_1^s \gtrsim 150M_\odot$, $q < 1$ systems have a comparatively larger observable volume than $q = 1$. This makes it relatively more important to include HM for detecting these high-mass IMBH systems. **Right panel:** Improvement in the sensitivity volume with the IAS – HM pipeline compared to IAS – 22 pipeline for different q against the source-frame total mass. The dashed horizontal line at $\overline{VT}_{\text{HM}}/\overline{VT}_{22} = 1$ indicates no gain or loss in the sensitivity volume. Note that the improvement exceeds 100% (i.e., by a factor of 2) around $M_{\text{tot}}^s \sim 320 M_\odot$ ($m_1^s \sim 250 M_\odot$) for $q = 1/4$.

$\sim 60 M_\odot$, the median improvement in sensitivity volume reaches approximately $\Delta\overline{VT} \sim 15\%$.

Comparison of IAS and LVK pipelines: The IAS pipelines for $q = 1$ perform comparably to the two main LVK pipelines, `gstLAL` and `pycbc_bbh` (despite the absence of Virgo data in the IAS analysis). It is worth mentioning that the injection set also contains the optimistic LVK-Any case, based on injections which clear $p_{\text{astro}} > 0.5$ in either of the LVK pipelines. We leave further discussion of this case to the supplemental material.

Sensitivity volume for BBH + IMBH injection sets

We will now discuss the results shown in Fig. 2 for the injection set containing a combination of BBH and IMBH sets using the “mixture model” available on Zenodo [68]. We considered mean mass ratios $q = 1$ and $q = 1/4$, and took the width of the log-normal distribution to be 0.15 to have a healthy N_{eff} in Eq. (6). For the IMBH injection set, only the `pycbc_bbh` results are available among the LVK pipelines, and the analysis provides only the IFAR for its recorded injections. We, therefore, adopt a cut on IFAR to set the detection criterion for \overline{VT} calculations, enabling a fair comparison with the IAS pipelines. We choose $\text{IFAR} > 1$ year consistent with the threshold used for the population analysis of BHs in GWTC-3 [21].

The trends in Fig. 2 at lower masses closely resemble those in Fig. 1, as expected. For $q = 1$, the IAS – 22 and `pycbc_bbh` pipelines exhibit similar sensi-

tivity volumes for m_1^s below $\sim 130 M_\odot$. However, beyond this threshold, the IAS – 22 pipeline significantly outperforms `pycbc_bbh`, with the sensitivity volume for `pycbc_bbh` dropping to near zero beyond $m_1^s \sim 200 M_\odot$ (corresponding to $M_{\text{tot}}^s \sim 400 M_\odot$). This decline can be attributed to the `pycbc_bbh` pipeline’s use of a lower threshold on template duration, set at 0.15 s during the search analysis [19, 71]. Signals from systems with $M_{\text{tot}}^s \gtrsim 400 M_\odot$ have durations much shorter than this threshold, leading to a loss of sensitivity. For a lower mass ratio, $q = 1/4$, the IAS – 22 and `pycbc_bbh` pipelines demonstrate comparable sensitivity volumes up to a relatively higher m_1^s (as $M_{\text{tot}}^s \sim 400 M_\odot$ corresponds to $m_1^s \sim 300 M_\odot$).

Having higher M_{tot} in the IMBH range can worsen detectability as the signal starts to shift out of the detector band ($f_{\text{min}} \sim 20$ Hz). As seen in Fig. 2, this effect leads to favoring the detectability of $q < 1$ systems over equal mass-ratio systems beyond $m_1^s \gtrsim 150M_\odot$ (as $q < 1$ systems have a lower M_{tot}^s at given m_1^s).

The right panel of Fig. 2 characterizes the improvement in sensitivity volume ($\overline{VT}_{\text{HM}}/\overline{VT}_{22}$) upon including HM. As both the total mass and inverse mass ratio ($1/q$) of binary mergers increase, the contribution of HM to the signal becomes more significant (see Fig.1 of [24] and also [25–35]). Indeed, the figure shows a clear trend of increasing fractional improvements with higher total masses for all mass ratios. For $q = 1/4$, the inclusion of HM results in substantial sensitivity gains, with sensi-

tivity volumes increasing by $\sim 15\% - 150\%$ for primary masses in the range $\sim [100, 250] M_{\odot}$, corresponding to total masses of $\sim [125, 330] M_{\odot}$.

It is worth noting that, beyond a certain total mass, the improvements begin to decline for all q . This could be due to incompleteness in IAS template banks (only binaries till detector-frame total mass, $M_{\text{tot}} \leq 400 M_{\odot}$ are currently included [24]), and glitches dominating the background at high masses [1]. We leave a detailed analysis of this effect to a future study. We omitted the cases $q < 1/4$ and $M_{\text{tot}}^s > 500 M_{\odot}$, as the injection set has insufficient N_{eff} , resulting in large uncertainties in \bar{VT} and $\Delta\bar{VT}$.

CONCLUSIONS

We investigated the impact of incorporating HM into the search pipelines for GW detections. We utilized injection datasets made available by the LVK collaboration for calculating the sensitivity volume-time (\bar{VT}) of different pipelines. We compared the following cases: IAS pipelines with and without including higher harmonics in the search templates; and various LVK pipelines (all of which currently only include the (2,2) mode in their templates).

For high-mass and/or unequal-mass-ratio binaries, addition of HM leads to a significant improvement in sensitivity volume (Figs. 1 and 2). The gains are particularly noteworthy in the high-mass range, enhancing \bar{VT} by $\sim 15\% - 150\%$ for binaries with the primary source mass, $m_1^s \sim [100, 250] M_{\odot}$. For nearly equal mass-ratio binaries, we find that including HM in our search does not lead to degradation of sensitivity. This is likely due to the fact that we use a marginalized detection statistic to upweight systems with larger observable volumes (e.g., $q \sim 1$ systems) and vice versa. We also show that the IAS pipeline with HM (IAS – HM) has sensitive volume better than or comparable to that of individual LVK pipelines across the entire range of binary parameter space we probed.

We showed results corresponding to the IAS – HM pipeline^a in this paper, but we expect our sensitivity results to also hold for other search pipelines if HM are introduced using the mode-by-mode filtering method. We provide the updated LVK injection summary files containing our IAS – HM and IAS – 22 results on Zenodo [72].

ACKNOWLEDGEMENTS

We thank Sharan Banagiri, Aaron Zimmerman, Will Farr and Maya Fishbach for useful discussions. DW gratefully acknowledges support from the Friends of the Institute for Advanced Study Membership and the Keck foundation. TV acknowledges support from NSF grants

2012086 and 2309360, the Alfred P. Sloan Foundation through grant number FG-2023-20470, the BSF through award number 2022136 and the Hellman Family Faculty Fellowship. BZ is supported by the Israel Science Foundation, NSF-BSF and by a research grant from the Willner Family Leadership Institute for the Weizmann Institute of Science. MZ is supported by NSF 2209991 and NSF-BSF 2207583 and by the Nelson Center for Collaborative Research. This research was also supported in part by the National Science Foundation under Grant No. NSF PHY-1748958. We also thank ICTS-TIFR for their hospitality during the completion of a part of this work.

This research has made use of data, software and/or web tools obtained from Zenodo [68] and the Gravitational Wave Open Science Center (<https://www.gw-openscience.org/>), a service of LIGO Laboratory, the LIGO Scientific Collaboration and the Virgo Collaboration. LIGO Laboratory and Advanced LIGO are funded by the United States National Science Foundation (NSF) as well as the Science and Technology Facilities Council (STFC) of the United Kingdom, the Max-Planck-Society (MPS), and the State of Niedersachsen/Germany for support of the construction of Advanced LIGO and construction and operation of the GEO600 detector. Additional support for Advanced LIGO was provided by the Australian Research Council. Virgo is funded, through the European Gravitational Observatory (EGO), by the French Centre National de Recherche Scientifique (CNRS), the Italian Istituto Nazionale di Fisica Nucleare (INFN) and the Dutch Nikhef, with contributions by institutions from Belgium, Germany, Greece, Hungary, Ireland, Japan, Monaco, Poland, Portugal, Spain.

Supplemental material

Updates to 22-only IAS pipeline

The 22-only pipeline we used in this paper (IAS – 22) is the limit of the IAS – HM pipeline when higher harmonics are turned off (i.e., the SNR in the (3,3) and (4,4) modes is set to zero). Note that the IAS – 22 case in this paper is different from the previous version of the 22-only IAS pipeline which was used to produce the IAS O3a and O3b catalogs in Refs. [17], [11]. The IAS – 22 case includes all the improvements that we made for the IAS – HM search listed in Refs. [24] and [1] (except, of course, the inclusion of HM). For the template banks, we use random forest regressor increase the efficiency of the banks (see Fig. 1 of Ref. [24]). We also use band eraser to remove excess noise (see Fig. 4 of Ref. [1]). We use exactly the same astrophysical prior in the IAS – HM and IAS – 22 searches so one can compare the pipelines directly. Unlike the previous version of astrophysical prior

used in Refs. [17], [11], our astrophysical prior includes the information of the observable volume of binaries, e.g., it upweights systems with positive effective spin (χ_{eff}) compared to negative χ_{eff} [20].

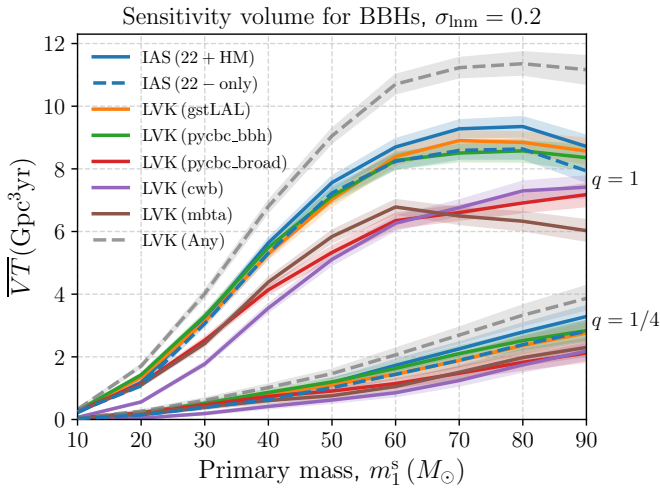


FIG. 3: Similar to Fig. 1 in the main text, but including the special LVK-Any case in dotted and including both $q = 1$ and $q = 1/4$ cases. LVK-Any is an optimistic estimate which combines only the detected injections from all the LVK pipelines (without accounting for an increase in the overall background due to the look-elsewhere effect), see the text for details.

Volume sensitivity plot including LVK – Any

In Fig. 1 of the main text of the paper, we had compared the volume-time \overline{VT} sensitivity of the IAS and LVK pipelines. Here, in Fig. 3, we show \overline{VT} for the additional case labeled as LVK-Any. This case considers a trigger (or injection) in the LVK detectors as detected if any of the five LVK pipelines shown in the legend assigns it a value $p_{\text{astro}} > 0.5$. As expected, the combined \overline{VT} is larger than that of the individual LVK pipelines, as seen in the dotted lines in Fig. 3. However, this procedure will also allow for additional background (as a statistic that maximizes over p_{astro} among pipelines would also produce a larger number of background triggers above a p_{astro} value than the individual pipelines). See Refs. [73, 74] for further discussion, where they also propose statistically consistent ways to combine pipelines by reweighting the individual p_{astro} values.

[1] D. Wadekar, T. Venumadhav, J. Roulet, A. K. Mehta, B. Zackay, J. Mushkin, and M. Zaldarriaga, *Phys. Rev. D* **110**, 044063 (2024), arXiv:2405.17400 [gr-qc].

- [2] J. Aasi *et al.* (LIGO Scientific), *Class. Quant. Grav.* **32**, 074001 (2015), arXiv:1411.4547 [gr-qc].
- [3] F. Acernese *et al.* (VIRGO), *Class. Quant. Grav.* **32**, 024001 (2015), arXiv:1408.3978 [gr-qc].
- [4] T. Akutsu *et al.* (KAGRA), *PTEP* **2021**, 05A101 (2021), arXiv:2005.05574 [physics.ins-det].
- [5] K. Cannon, S. Caudill, C. Chan, B. Cousins, *et al.*, *SoftwareX* **14**, 100680 (2021).
- [6] F. Aubin *et al.*, *Class. Quant. Grav.* **38**, 095004 (2021), arXiv:2012.11512 [gr-qc].
- [7] S. Klimentenko *et al.*, *Phys. Rev. D* **93**, 042004 (2016), arXiv:1511.05999 [gr-qc].
- [8] S. A. Usman *et al.*, *Class. Quant. Grav.* **33**, 215004 (2016), arXiv:1508.02357 [gr-qc].
- [9] T. Venumadhav, B. Zackay, J. Roulet, L. Dai, and M. Zaldarriaga, *Phys. Rev. D* **100**, 023011 (2019), arXiv:1902.10341 [astro-ph.IM].
- [10] T. Venumadhav, B. Zackay, J. Roulet, L. Dai, and M. Zaldarriaga, *Phys. Rev. D* **101**, 083030 (2020), arXiv:1904.07214 [astro-ph.HE].
- [11] S. Olsen, T. Venumadhav, J. Mushkin, J. Roulet, B. Zackay, and M. Zaldarriaga, *Phys. Rev. D* **106**, 043009 (2022).
- [12] A. H. Nitz, C. Capano, A. B. Nielsen, S. Reyes, R. White, D. A. Brown, and B. Krishnan, *The Astrophysical Journal* **872**, 195 (2019).
- [13] A. H. Nitz, T. Dent, G. S. Davies, S. Kumar, *et al.*, *Astrophys. J.* **891**, 123 (2020), arXiv:1910.05331 [astro-ph.HE].
- [14] A. H. Nitz, C. D. Capano, S. Kumar, Y.-F. Wang, *et al.*, *arXiv e-prints*, arXiv:2105.09151 (2021), arXiv:2105.09151 [astro-ph.HE].
- [15] A. H. Nitz, S. Kumar, Y.-F. Wang, S. Kastha, *et al.*, “4-OGC: Catalog of gravitational waves from compact-binary mergers,” (2021), arXiv:2112.06878 [astro-ph.HE].
- [16] H. S. Chia, T. D. P. Edwards, D. Wadekar, A. Zimmerman, *et al.*, *Phys. Rev. D* **110**, 063007 (2024), arXiv:2306.00050 [gr-qc].
- [17] A. K. Mehta, S. Olsen, D. Wadekar, J. Roulet, *et al.*, *arXiv e-prints*, arXiv:2311.06061 (2023), arXiv:2311.06061 [gr-qc].
- [18] A. E. Koloniari, E. C. Koursoumpa, P. Nousi, P. Lampropoulos, N. Passalis, A. Tefas, and N. Stergioulas, *arXiv e-prints*, arXiv:2407.07820 (2024), arXiv:2407.07820 [gr-qc].
- [19] R. Abbott *et al.* (LIGO Scientific, VIRGO, KAGRA), (2021), arXiv:2111.03606 [gr-qc].
- [20] D. Wadekar, J. Roulet, T. Venumadhav, A. K. Mehta, *et al.*, *arXiv e-prints*, arXiv:2312.06631 (2023), arXiv:2312.06631 [gr-qc].
- [21] R. Abbott *et al.* (KAGRA, VIRGO, LIGO Scientific), *Phys. Rev. X* **13**, 011048 (2023), arXiv:2111.03634 [astro-ph.HE].
- [22] J. Roulet, H. S. Chia, S. Olsen, L. Dai, T. Venumadhav, B. Zackay, and M. Zaldarriaga, *Phys. Rev. D* **104**, 083010 (2021).
- [23] R. Abbott *et al.* (LIGO Scientific, VIRGO, KAGRA), (2021), arXiv:2112.06861 [gr-qc].
- [24] D. Wadekar, T. Venumadhav, A. K. Mehta, J. Roulet, *et al.*, *arXiv e-prints*, arXiv:2310.15233 (2023), arXiv:2310.15233 [gr-qc].
- [25] L. Pekowsky, J. Healy, D. Shoemaker, and P. Laguna, *Physical Review D* **87** (2013), 10.1103/phys-

- revd.87.084008.
- [26] J. Healy, P. Laguna, L. Pekowsky, and D. Shoemaker, *Physical Review D* **88** (2013), 10.1103/physrevd.88.024034.
- [27] C. Capano, Y. Pan, and A. Buonanno, *Physical Review D* **89** (2014), 10.1103/physrevd.89.102003.
- [28] J. C. Bustillo, S. Husa, A. M. Sintes, and M. Pürrer, *Physical Review D* **93** (2016), 10.1103/physrevd.93.084019.
- [29] J. C. Bustillo, P. Laguna, and D. Shoemaker, *Physical Review D* **95** (2017), 10.1103/physrevd.95.104038.
- [30] J. C. Bustillo, F. Salemi, T. D. Canton, and K. P. Jani, *Physical Review D* **97** (2018), 10.1103/physrevd.97.024016.
- [31] C. Mills and S. Fairhurst, *Phys. Rev. D* **103**, 024042 (2021), arXiv:2007.04313 [gr-qc].
- [32] I. Harry, J. C. Bustillo, and A. Nitz, *Phys. Rev. D* **97**, 023004 (2018).
- [33] K. Chandra, J. Calderón Bustillo, A. Pai, and I. Harry, arXiv e-prints, arXiv:2207.01654 (2022), arXiv:2207.01654 [gr-qc].
- [34] K. Sharma, K. Chandra, and A. Pai, arXiv e-prints, arXiv:2208.02545 (2022), arXiv:2208.02545 [astro-ph.HE].
- [35] C. Zhang, N. Dai, and D. Liang, *Phys. Rev. D* **108**, 044076 (2023), arXiv:2306.13871 [gr-qc].
- [36] R. Abbott *et al.* (LIGO Scientific, VIRGO, KAGRA), *Astron. Astrophys.* **659**, A84 (2022), arXiv:2105.15120 [astro-ph.HE].
- [37] M. COLEMAN MILLER and E. J. M. COLBERT, *International Journal of Modern Physics D* **13**, 1 (2004), <https://doi.org/10.1142/S0218271804004426>.
- [38] J. R. Gair, I. Mandel, M. C. Miller, and M. Volonteri, *General Relativity and Gravitation* **43**, 485 (2011), arXiv:0907.5450 [astro-ph.CO].
- [39] R. Abbott, LIGO Scientific Collaboration, and Virgo Collaboration, *Phys. Rev. D* **102**, 043015 (2020), arXiv:2004.08342 [astro-ph.HE].
- [40] R. Abbott *et al.*, *Astrophys. J. Lett.* **896**, L44 (2020), arXiv:2006.12611 [astro-ph.HE].
- [41] O. Anagnostou, M. Trenti, and A. Melatos, (2020), arXiv:2010.06161 [astro-ph.HE].
- [42] G. Fragione, A. Loeb, and F. A. Rasio, *Astrophys. J. Lett.* **902**, L26 (2020), arXiv:2009.05065 [astro-ph.GA].
- [43] D. Veske, A. G. Sullivan, Z. Márka, I. Bartos, *et al.*, *Astrophys. J. Lett.* **907**, L48 (2021), arXiv:2011.06591 [astro-ph.HE].
- [44] G. Fragione, B. Kocsis, F. A. Rasio, and J. Silk, (2021), arXiv:2107.04639 [astro-ph.GA].
- [45] Y. Yang, I. Bartos, V. Gayathri, K. E. S. Ford, *et al.*, *Phys. Rev. Lett.* **123**, 181101 (2019).
- [46] B. McKernan, K. E. S. Ford, R. O’Shaughnessy, and D. Wysocki, *Monthly Notices of the Royal Astronomical Society* **494**, 1203 (2020), <https://academic.oup.com/mnras/article-pdf/494/1/1203/33029648/staa740.pdf>.
- [47] H. Tagawa, Z. Haiman, I. Bartos, and B. Kocsis, *The Astrophysical Journal* **899**, 26 (2020).
- [48] Ishibashi, W. and Gröbner, M., *A&A* **639**, A108 (2020).
- [49] A. Secunda, J. Bellovary, M.-M. Mac Low, K. E. S. Ford, *et al.*, *Astrophys. J.* **903**, 133 (2020), arXiv:2004.11936 [astro-ph.HE].
- [50] H. Tagawa, B. Kocsis, Z. Haiman, I. Bartos, K. Omukai, and J. Samsing, *Astrophys. J.* **908**, 194 (2021), arXiv:2012.00011 [astro-ph.HE].
- [51] G. Fabj, S. S. Nasim, F. Caban, K. E. S. Ford, B. McKernan, and J. M. Bellovary, *Mon. Not. Roy. Astron. Soc.* **499**, 2608 (2020), arXiv:2006.11229 [astro-ph.GA].
- [52] H. Tagawa, Z. Haiman, I. Bartos, and B. Kocsis, *Astrophys. J.* **899**, 26 (2020), arXiv:2004.11914 [astro-ph.HE].
- [53] J. Samsing, I. Bartos, D. J. D’Orazio, Z. Haiman, *et al.*, *Nature (London)* **603**, 237 (2022), arXiv:2010.09765 [astro-ph.HE].
- [54] P. Marchant and T. Moriya, *Astron. Astrophys.* **640**, L18 (2020), arXiv:2007.06220 [astro-ph.HE].
- [55] R. Farmer, M. Renzo, S. E. de Mink, P. Marchant, and S. Justham, (2019), 10.3847/1538-4357/ab518b, arXiv:1910.12874 [astro-ph.SR].
- [56] L. A. C. van Son, S. E. De Mink, F. S. Broekgaarden, M. Renzo, *et al.*, *Astrophys. J.* **897**, 100 (2020), arXiv:2004.05187 [astro-ph.HE].
- [57] A. K. Mehta, A. Buonanno, J. Gair, M. C. Miller, *et al.*, *Astrophys. J.* **924**, 39 (2022), arXiv:2105.06366 [gr-qc].
- [58] D. D. Hendriks, L. A. C. van Son, M. Renzo, R. G. Izzard, and R. Farmer, *Mon. Not. R. Astron. Soc.* (2023), 10.1093/mnras/stad2857, arXiv:2309.09339 [astro-ph.HE].
- [59] J. Golomb, M. Isi, and W. Farr, arXiv e-prints, arXiv:2312.03973 (2023), arXiv:2312.03973 [astro-ph.HE].
- [60] G. Franciolini, K. Kritos, L. Reali, F. Broekgaarden, and E. Berti, arXiv e-prints, arXiv:2401.13038 (2024), arXiv:2401.13038 [astro-ph.HE].
- [61] G. Fragione, I. Ginsburg, and B. Kocsis, *Astrophys. J.* **856**, 92 (2018), arXiv:1711.00483 [astro-ph.GA].
- [62] K. Kritos, E. Berti, and J. Silk, *Phys. Rev. D* **108**, 083012 (2023), arXiv:2212.06845 [astro-ph.HE].
- [63] K. Kritos, L. Reali, D. Gerosa, and E. Berti, *Phys. Rev. D* **110**, 123017 (2024), arXiv:2409.15439 [astro-ph.HE].
- [64] K. Kritos, V. Stokov, V. Baibhav, and E. Berti, *Phys. Rev. D* **110**, 043023 (2024), arXiv:2210.10055 [astro-ph.HE].
- [65] K. Chandra, V. Gayathri, J. Calderon Bustillo, and A. Pai, arXiv e-prints, arXiv:2002.10666 (2020), arXiv:2002.10666 [astro-ph.CO].
- [66] S. Fairhurst, C. Hoy, R. Green, C. Mills, and S. A. Usman, *Phys. Rev. D* **108**, 082006 (2023), arXiv:2304.03731 [gr-qc].
- [67] J. Roulet, J. Mushkin, D. Wadekar, T. Venumadhav, B. Zackay, and M. Zaldarriaga, arXiv e-prints, arXiv:2404.02435 (2024), arXiv:2404.02435 [gr-qc].
- [68] K. C. LIGO Scientific Collaboration, Virgo Collaboration, (2021), 10.5281/zenodo.5546675.
- [69] V. Tiwari, *Class. Quant. Grav.* **35**, 145009 (2018), arXiv:1712.00482 [astro-ph.HE].
- [70] W. M. Farr, *Research Notes of the AAS* **3**, 66 (2019).
- [71] T. Dal Canton and I. W. Harry, (2017), arXiv:1705.01845 [gr-qc].
- [72] A. K. Mehta, (2024), 10.5281/zenodo.14752873.
- [73] S. Banagiri, C. P. L. Berry, G. S. Cabourn Davies, L. Tsukada, and Z. Doctor, *Phys. Rev. D* **108**, 083043 (2023), arXiv:2305.00071 [astro-ph.IM].
- [74] R. Biswas *et al.*, *Phys. Rev. D* **85**, 122009 (2012), arXiv:1201.2964 [gr-qc].